IOPscience iopscience.iop.org

Home Search Collections Journals About Contact us My IOPscience

Requirements for contractility in disordered cytoskeletal bundles

This article has been downloaded from IOPscience. Please scroll down to see the full text article.

2012 New J. Phys. 14 033037

(http://iopscience.iop.org/1367-2630/14/3/033037)

View the table of contents for this issue, or go to the journal homepage for more

Download details:
IP Address: 67.174.141.250
The article was downloaded on 29/03/2012 at 04:52

Please note that terms and conditions apply.

New Journal of Physics
The open-access journal for physics

Requirements for contractility in disordered cytoskeletal bundles

Martin Lenz[1,4], **Margaret L Gardel**[1,2,3] **and Aaron R Dinner**[1,2,3]
[1] James Franck Institute, University of Chicago, Chicago, IL 60637, USA
[2] Institute for Biophysical Dynamics, University of Chicago, Chicago, IL 60637, USA
[3] Department of Physics, University of Chicago, Chicago, IL 60637, USA
E-mail: martinlenz@uchicago.edu

New Journal of Physics **14** (2012) 033037 (17pp)
Received 22 October 2011
Published 28 March 2012
Online at http://www.njp.org/
doi:10.1088/1367-2630/14/3/033037

Abstract. Actomyosin contractility is essential for biological force generation, and is well understood in highly organized structures such as striated muscle. Additionally, actomyosin bundles devoid of this organization are known to contract both *in vivo* and *in vitro*, which cannot be described by standard muscle models. To narrow down the search for possible contraction mechanisms in these systems, we investigate their microscopic symmetries. We show that contractile behavior requires non-identical motors that generate large-enough forces to probe the nonlinear elastic behavior of F-actin. This suggests a role for filament buckling in the contraction of these bundles, consistent with recent experimental results on reconstituted actomyosin bundles.

[4] Author to whom any correspondence should be addressed.

© IOP Publishing Ltd and Deutsche Physikalische Gesellschaft

Contents

1. Introduction

The large-scale motion of living organisms often depends on their ability to harness the power of nanometer-sized molecular motors to generate macroscopic displacements. For instance, our striated muscles rely on clusters—or 'thick filaments'—of the molecular motor myosin to generate forces. Myosin thick filaments are able to slide directionally toward the barbed end of polar actin filaments (F-actin), and the characteristic organization of striated muscles into periodic sarcomeres arranged in series allows the transfer of this microscopic motion to larger scales (figure 1(a)) [1].

Despite its familiarity, sarcomere-like organization is far from a universal feature of contractile actomyosin assemblies. In some instances, partially periodic arrangements reminiscent of sarcomeres are observed, as in subcellular contractile bundles known as stress fibers [2]. In many other cases, however, no such organization is known to exist. Examples include smooth muscle fibers [3], transverse arcs [4], graded polarity bundles [5], the cell cortex [6] and lamellar networks [7]. Sarcomere-like contraction is unlikely to apply to these systems, and there is no consensus regarding their actual deformation mechanism.

In vitro experiments using purified proteins are useful in understanding contraction in these systems and have been used to identify the minimum requirements for actomyosin contractility since the 1940s [8]. Modern attempts using dilute actomyosin gels were not able to induce contractility in the presence of actin and myosin alone, although adding the actin cross-linker α-actinin did produce observable contraction [9–12]. However, a more recent study using denser actomyosin bundles shows that F-actin and myosin can induce contractility on their own [13]. Unlike in sarcomeres, in these bundles F-actin lacks polarity ordering, and myosins are not aligned in register. We therefore refer to them as 'disordered'.

Previous theoretical work on disordered actomyosin systems include continuum models focused on length scales much larger than an individual actin filament [14–17]. In these elegant descriptions, contractility is introduced phenomenologically, which circumvents the question of its emergence from microscopic interactions. Several other studies do, however, investigate this connection. In simulations without sarcomeric organization or cross-linkers, thick filaments simply sort F-actin by polarity without inducing any overall contraction [18]. To restore

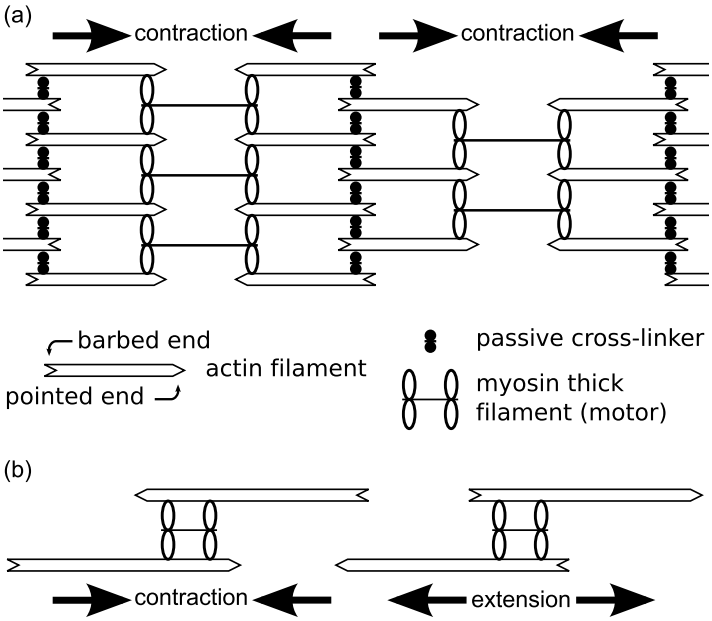

Figure 1. Contraction and extension in actomyosin systems. (a) Contraction in sarcomeres occurs as motors localized in the vicinity of the F-actin pointed ends slide toward F-actin barbed ends. (b) A motor located near the F-actin pointed ends induces local contraction as in sarcomeres (left), whereas localization near the barbed ends yields extension (right). The two effects balance each other in a large class of bundles, which we characterize in this paper.

contractility, several models assume that thick filaments tend to dwell at the barbed end of F-actin after sliding over its whole length [19–22] or more generally that their velocity depends on their position relative to the filament [23]. In these models, F-actin tend to have immobilized motors that transiently act as passive cross-linkers at their barbed ends. This essentially introduces a small amount of sarcomere-like organization and results in contractility [18]. However, no direct experimental evidence for thick filaments dwelling at the barbed end of F-actin is available.

Here we investigate the possibility for bundle contraction in the absence of any sarcomeric organization, including motors dwelling at the filament barbed ends. After introducing a general bundle model in section 2, we show in section 3 that underlying symmetries between contraction and extension (figure 1(b)) imply that disordered bundle contraction requires non-identical motors and nonlinear elastic behavior of the filaments. Intuitively, non-identical motors induce mechanical frustration in a disordered actomyosin bundle, thus generating both contractile and extensile stresses. The filament nonlinear behavior then allows the former to deform the bundle while resisting the latter, yielding overall contraction. Finally, in section 4 we discuss the limitations of our model and propose a minimal model for the contraction of a non-sarcomeric bundle.

2. Bundle model

In order to make general statements about a disordered bundle of potentially complex internal geometry, we develop a detailed description of its mechanics without resorting to the simplifying

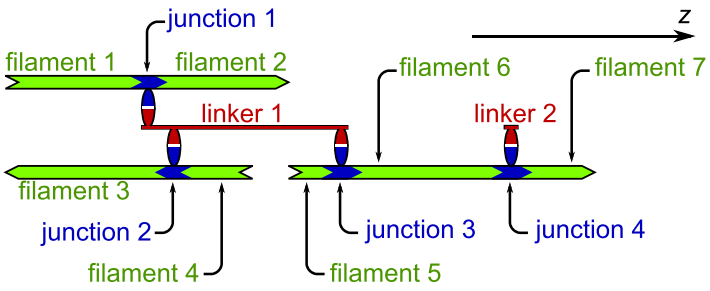

Figure 2. Schematic representation of a model bundle comprising three F-actin, one myosin thick filament bound in three different sites (linker 1) and one bound only once (linker 2). Colors indicate the division into linker units (red), junction units (blue) and filament units (green). Our model does not impose any restrictions on the number of junctions associated with a linker, whether they involve one or more F-actin, or the polarity of the F-actin.

mean-field approximations widely used in previous studies [19–23]. The main assumptions of our model are as follows. Firstly, we assume that the velocity of a motor only depends on the force applied to it by the F-actin to which it is bound. Secondly, the average deformation of a thermally fluctuating section of filament in the bundle only depends on the force applied longitudinally at its ends. Thirdly, we consider a stabilized bundle where F-actin polymerization and depolymerization do not occur. Finally, our model does not include the attachment–detachment dynamics of motors and cross-linkers to F-actin. The relevance of these choices is discussed in section 4.

We describe a bundle of arbitrary geometry by subdividing it into interacting 'units' of three types characterized by their lengths, velocities and tensions (section 2.1). Introducing general notations to describe the physical connections between different units, we express the relationships between their forces and velocities as a function of their spatial arrangement (section 2.2). The central physics of bundle mechanics are then described by introducing the filament force–extension relationships and the motor force–velocity relationships (section 2.3). Conservation equations are then used to derive a compact description of the bundle amenable to further discussion (section 2.4).

2.1. Linkers, filaments and junctions

Here we consider a single bundle constituted by F-actin, thick filaments of myosin molecular motors and optionally passive actin cross-linkers. F-actin are assumed to be aligned in the z-direction, and for simplicity we refer to the direction of positive (negative) z as the 'right' ('left') in the following. To describe the bundle, we decompose it so as to distinguish three types of 'units' (figure 2):

- **Linker units**, representing a whole myosin thick filament or a passive actin cross-linker (passive cross-linkers are equivalent to immobile motors). The total number of linker units in the system is denoted by n''.
- **Junction units**, representing the point of contact between a myosin thick filament or passive actin cross-linker, on the one hand, and an F-actin, on the other. The total number of junction units in the system is denoted by n'.

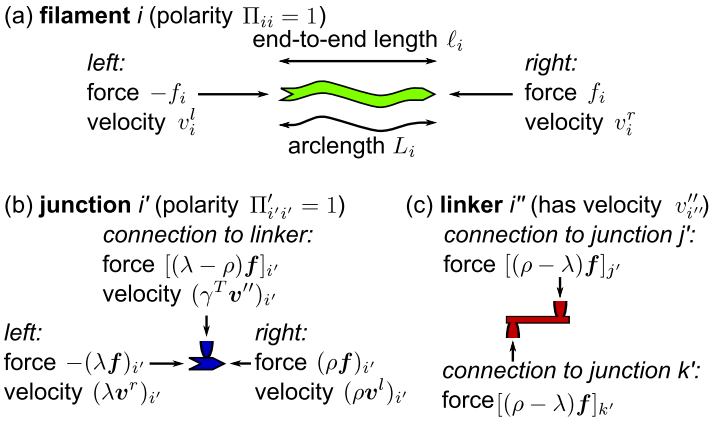

Figure 3. Summary of the notation. A filament unit (a), junction unit (b) and linker unit (c) are represented, along with the velocities and lengths characterizing their state, as well as the forces they are subjected to.

- **Filament units**, representing a *portion* of an F-actin comprised between two junction units or between one junction unit and an F-actin-free end. We do not consider freely floating F-actin (filament units with two free ends). The total number of filament units in the system is denoted by n.

We label the filament units as $i = 1, \ldots, n$, and denote by f_i the tension of filament unit i ($f_i > 0$ for a filament unit under extension). We allow filament units to bend away from the z-axis while maintaining their overall z-orientation, and thus introduce filament unit i's contour length and end-to-end length as two independent variables L_i and ℓ_i, respectively. Finally, we introduce the velocity v_i^{r} of the rightmost monomer of filament unit i, and the velocity v_i^{l} of its leftmost monomer. These two velocities are Eulerian velocities; in that respect, one might think of junction 1 of figure 2 as a bridge and the actin as the water that flows under it. Then the velocities v_1^{r} and v_2^{l} associated with filament units 1 and 2 are the velocities of the water just upstream and downstream of the bridge, as opposed to being the velocities of a specific fluid element. The notation is summarized in figure 3(a).

We label junction units as $i' = 1, \ldots, n'$, and linker units as $i'' = 1, \ldots, n''$. We introduce the velocity $v''_{i''}$ of linker unit i'', i.e. the velocity of the bridge itself in our previous analogy. We choose to work in the reference frame where the center of mass of all linker units is motionless, which reads

$$\sum_{i''=1}^{n''} v''_{i''} = 0. \tag{1}$$

Note that the velocities v_i^{r} and v_i^{l} are absolute velocities defined in this reference frame, as opposed to being velocities relative to the neighboring linker. We delay labeling the other forces and velocities involved in junction and linker units until the introduction of convenient notations in the next section.

2.2. Bundle geometry and topology

To describe the physical connections between junction and filament units, we define the $n' \times n$ matrices ρ and λ by

$$\rho_{i'i} = \begin{cases} 1 & \text{if } i \text{ is the right-hand neighbor of } i', \\ 0 & \text{otherwise,} \end{cases} \tag{2a}$$

$$\lambda_{i'i} = \begin{cases} 1 & \text{if } i \text{ is the left-hand neighbor of } i', \\ 0 & \text{otherwise.} \end{cases} \tag{2b}$$

For instance, the bundle represented in figure 2 is described by

$$\lambda = \begin{pmatrix} 1 & 0 & 0 & 0 & 0 & 0 & 0 \\ 0 & 0 & 1 & 0 & 0 & 0 & 0 \\ 0 & 0 & 0 & 0 & 1 & 0 & 0 \\ 0 & 0 & 0 & 0 & 0 & 1 & 0 \end{pmatrix}, \qquad \rho = \begin{pmatrix} 0 & 1 & 0 & 0 & 0 & 0 & 0 \\ 0 & 0 & 0 & 1 & 0 & 0 & 0 \\ 0 & 0 & 0 & 0 & 0 & 1 & 0 \\ 0 & 0 & 0 & 0 & 0 & 0 & 1 \end{pmatrix}. \tag{3}$$

The usefulness of these matrices is illustrated by introducing the notation $\boldsymbol{f} = (f_1, \ldots, f_n)$ for the vector of all filament tensions, as well as similar notations $\boldsymbol{L}$, $\boldsymbol{\ell}$, $\boldsymbol{v}^{\mathrm{r}}$, $\boldsymbol{v}^{\mathrm{l}}$, $\boldsymbol{v}''$. The matrix product $\rho\boldsymbol{f}$ is a vector of length n' whose i'th component $(\rho\boldsymbol{f})_{i'}$ is the tension of the filament unit that is the right-hand neighbor of junction unit i'. This neighbor thus exerts a force $(\rho\boldsymbol{f})_{i'}$ on junction unit i', while its left-hand neighbor exerts $-(\lambda\boldsymbol{f})_{i'}$. The sum of these two forces is equal and opposite to the force applied to junction unit i' by its linker unit. This last force thus reads $[(\lambda - \rho)\boldsymbol{f}]_{i'}$ (figure 3(b)).

Further use of ρ and λ indicates that the velocities of the rightmost and leftmost actin monomers involved in junction unit i' are $(\rho\boldsymbol{v}^{\mathrm{l}})_{i'}$ and $(\lambda\boldsymbol{v}^{\mathrm{r}})_{i'}$, respectively (figure 3(b)). As junction units are point-like objects, the net actin flow in and out of them vanishes and

$$\lambda\boldsymbol{v}^{\mathrm{r}} = \rho\boldsymbol{v}^{\mathrm{l}}. \tag{4}$$

The reasoning used here can be generalized in the following way: if x_i is a quantity associated with filament i, then $(\rho\boldsymbol{x})_{i'}$ is associated with the right-hand neighbor of junction unit i'. For instance, in the two previous paragraphs we considered $x_i = f_i$ and $x_i = v_i^{\mathrm{l}}$ or v_i^{r}, respectively. Just as this statement relates junction units to quantities associated with the neighboring filament units, we can conversely relate filament units to quantities associated with their junction unit neighbors as follows. If $x'_{i'}$ is associated with junction unit i', then $(\rho^{\mathrm{T}}\boldsymbol{x}')_i$ is associated with the junction unit that is the *left* neighbor of filament unit i if it has one, or is equal to zero if it does not (the superscript T denotes the matrix transpose). A similar statement holds for λ^{T}. Combining this with the fact that each junction unit has exactly one right-hand and one left-hand neighbor, we find that $(\rho\rho^{\mathrm{T}}\boldsymbol{x}')_{i'} = x'_{i'}$ always. More generally,

$$\rho\rho^{\mathrm{T}} = \lambda\lambda^{\mathrm{T}} = \mathbb{1}, \tag{5}$$

where $\mathbb{1}$ denotes the identity matrix. We further note that filament units may have one or two neighbors, which implies that

$$(\rho^{\mathrm{T}}\rho\boldsymbol{x})_i = \begin{cases} x_i & \text{if } i \text{ has a left-hand neighbor,} \\ 0 & \text{if it does not.} \end{cases} \tag{6}$$

This means that the matrix $\rho^{\mathrm{T}}\rho$ is a projector onto the subspace of filament units that have a left-hand neighbor. A similar statement holds for $\lambda^{\mathrm{T}}\lambda$. This discussion implies that $n' < n$.

To describe the polarity of the filament units, we introduce the diagonal $n \times n$ matrix Π, where $\Pi_{ii} = 1$ if the pointed end of filament unit i points to the right, and $\Pi_{ii} = -1$ if it points to the left. As an example, figure 2 has

$$\Pi = \mathrm{diag}(1, 1, -1, -1, 1, 1, 1). \tag{7}$$

A similar diagonal polarity matrix Π' is associated with junction units, and since neighboring filaments and junction units have the same polarity we have

$$\Pi' = \rho \Pi \rho^{\mathrm{T}} = \lambda \Pi \lambda^{\mathrm{T}}. \tag{8}$$

Turning to the linker units, we define the $n'' \times n'$ matrix γ by

$$\gamma_{i''i'} = \begin{cases} 1 & \text{if } i' \text{ is connected to } i'', \\ 0 & \text{otherwise.} \end{cases} \tag{9}$$

For instance, figure 2 has

$$\gamma = \begin{pmatrix} 1 & 1 & 1 & 0 \\ 0 & 0 & 0 & 1 \end{pmatrix}. \tag{10}$$

Therefore, the velocity of the linker unit connected to junction unit i' is $(\gamma^{\mathrm{T}} \boldsymbol{v}'')_{i'}$ (figure 3(b)). Each junction unit is connected to a linker unit, but one linker unit can be connected to several junction units, which implies that $n'' \leqslant n'$.

To obtain the forces associated with the linker units, we reason that if i' experiences a force $[(\lambda - \rho)\boldsymbol{f}]_{i'}$ from its linker unit, then i' exerts an equal and opposite force $[(\rho - \lambda)\boldsymbol{f}]_{i'}$ on the linker unit (figure 3(c)). Force balance imposes that the sum of the forces applied on any linker unit vanishes, and thus

$$\sum_{i' \text{ connected to } i''} [(\rho - \lambda)\boldsymbol{f}]_{i'} = 0, \tag{11}$$

or, in vector notation,

$$\gamma(\rho - \lambda)\boldsymbol{f} = 0. \tag{12}$$

Although this condition comprises n'' scalar equations, those equations are not all independent. This can be seen by considering the mechanical subsystem formed by all junction and filament units (but not including the linker units). As inertia and friction against the background fluid are negligible, the sum of all forces applied to this system by junction units must vanish:

$$\sum_{i'=1}^{n'} [(\lambda - \rho)\boldsymbol{f}]_{i'} = -\sum_{i''=1}^{n''} [\gamma(\rho - \lambda)\boldsymbol{f}]_{i''} = 0, \tag{13}$$

where the first equality follows from the fact that γ has exactly one element equal to 1 per column and zeros everywhere else. As equation (13) is always trivially true, equation (12) expresses only $n'' - 1$ linearly independent scalar conditions.

2.3. Filament elasticity and motor operation

Having defined notations for all lengths, forces and velocities in our system (figure 3) and having enforced the velocity continuity and force balance conditions, we turn to characterizing the more substantial physics of the junction and filament units.

Filament units are sections of semiflexible polymers shorter than or with a length comparable to their persistence length. We thus assume that the force required to hold a filament unit of a given contour length L_i in mechanical equilibrium is uniquely determined by specifying its end-to-end length ℓ_i, which defines the force–extension relationship F:

$$f_i = F(\ell_i, L_i). \tag{14}$$

In the case of a thermally fluctuating polymer, ℓ_i denotes the end-to-end length averaged over thermal fluctuations. Thermal bending of the filament unit, moreover, implies that ℓ_i is smaller than L_i even when $f_i = 0$. Since filament units are shorter than the filament persistence length, we expect deformations of this kind ranging from zero to $\approx$20%. In vector notation, we write

$$\boldsymbol{f} = \boldsymbol{F}(\boldsymbol{\ell}, \boldsymbol{L}). \tag{15}$$

Motor operation at junction i' is described by a functional relationship between the local velocity of the linker relative to the F-actin and the force applied to i':

$$(\rho \boldsymbol{v}^{\mathrm{l}} - \gamma^{\mathrm{T}} \boldsymbol{v}'')_{i'} = \tilde{V}'_{i'} \{[(\lambda - \rho)\boldsymbol{f}]_{i'}\}, \tag{16}$$

where the function $\tilde{V}'_{i'}$ *a priori* depends on the polarity $\Pi'_{i'i'}$ of the junction unit. This dependence can be explicitly determined by noting that the force–velocity relationship must not depend on our arbitrary choice of the direction of positive z. Reversing this choice is equivalent to reversing the sign of all velocities, forces and polarities. The only way for equation (16) to be invariant under this transformation is to write

$$(\rho \boldsymbol{v}^{\mathrm{l}} - \gamma^{\mathrm{T}} \boldsymbol{v}'')_{i'} = \Pi'_{i'i'} V'_{i'} \left\{\Pi'_{i'i'}[(\lambda - \rho)\boldsymbol{f}]_{i'}\right\}, \tag{17}$$

where function $V'_{i'}$ is the force–velocity relationship of motor i', an *a priori* nonlinear function independent of Π'. In vector notation,

$$\rho \boldsymbol{v}^{\mathrm{l}} - \gamma^{\mathrm{T}} \boldsymbol{v}'' = \Pi' \boldsymbol{V}'[\Pi'(\lambda - \rho)\boldsymbol{f}]. \tag{18}$$

2.4. Dynamical equations for bundle deformation

To provide a kinematic description of bundle contraction and extension, we write the conservation of F-actin contour length. The rate of change in the contour length of a filament unit is directly related to the velocity at which the neighboring junction units slide relative to F-actin. If i has a neighboring junction unit on its right-hand side, the velocity of the linker unit there is $(\lambda^{\mathrm{T}}\gamma^{\mathrm{T}}\boldsymbol{v}'')_i$, and its sliding velocity relative to the actin is $(\lambda^{\mathrm{T}}\gamma^{\mathrm{T}}\boldsymbol{v}'' - \boldsymbol{v}^{\mathrm{r}})_i$. We rewrite this sliding velocity as $(\lambda^{\mathrm{T}}\gamma^{\mathrm{T}}\boldsymbol{v}'' - \lambda^{\mathrm{T}}\lambda\boldsymbol{v}^{\mathrm{r}})_i$, which is equal to the previous expression if i has a right-hand neighbor and to zero if it does not. Using a similar reasoning for the left-hand side, we obtain

$$\frac{\mathrm{d}\boldsymbol{L}}{\mathrm{d}t} = (\lambda^{\mathrm{T}}\gamma^{\mathrm{T}}\boldsymbol{v}'' - \lambda^{\mathrm{T}}\lambda\boldsymbol{v}^{\mathrm{r}}) - (\rho^{\mathrm{T}}\gamma^{\mathrm{T}}\boldsymbol{v}'' - \rho^{\mathrm{T}}\rho\boldsymbol{v}^{\mathrm{l}}). \tag{19}$$

The first (second) term on the right-hand side of this equation accounts for actin-linker sliding on the right-hand (left-hand) side of the filament units, and vanishes for the filament units that do not have a right-hand (left-hand) neighbor junction unit.

We describe the evolution of the end-to-end length of a filament unit in different ways, depending on whether it has two junction unit neighbors or a free end. In the former case,

$$\frac{\mathrm{d}\ell_i}{\mathrm{d}t} = \left(\lambda^{\mathrm{T}}\gamma^{\mathrm{T}}\boldsymbol{v}''\right)_i - \left(\rho^{\mathrm{T}}\gamma^{\mathrm{T}}\boldsymbol{v}''\right)_i, \tag{20}$$

where the two terms in the right-hand side are the absolute velocities of the right and left neighbors of i, respectively. To describe a filament unit with one free end, we first note that it has vanishing tension. If the contour length of the filament unit is known, its end-to-end length is given by its force–extension relation equation (14) with $f_i = 0$. Differentiating with respect to time, we obtain

$$\frac{\partial F}{\partial \ell}\frac{\mathrm{d}\ell_i}{\mathrm{d}t} + \frac{\partial F}{\partial L}\frac{\mathrm{d}L_i}{\mathrm{d}t} = 0. \tag{21}$$

Defining the diagonal matrices

$$\left(\frac{\partial \boldsymbol{F}}{\partial \boldsymbol{L}}\right)_{ij} = \frac{\partial f_i}{\partial L_j} = \delta_{ij}\frac{\partial F}{\partial L}(\ell_i, L_i), \tag{22a}$$

$$\left(\frac{\partial \boldsymbol{F}}{\partial \boldsymbol{\ell}}\right)_{ij} = \frac{\partial f_i}{\partial \ell_j} = \delta_{ij}\frac{\partial F}{\partial \ell}(\ell_i, L_i), \tag{22b}$$

where δ_{ij} is the Kronecker delta, we rewrite equation (21) as

$$\frac{\mathrm{d}\ell_i}{\mathrm{d}t} = -\left[\left(\frac{\partial \boldsymbol{F}}{\partial \boldsymbol{\ell}}\right)^{-1}\frac{\partial \boldsymbol{F}}{\partial \boldsymbol{L}}\frac{\mathrm{d}\boldsymbol{L}}{\mathrm{d}t}\right]_i \tag{23}$$

for a filament unit with a free end[5]. Making use of equation (6) and its analogue for $\lambda^{\mathrm{T}}\lambda$, we write an equation that describes filament units whether they have one or two neighboring junction units:

$$\frac{\mathrm{d}\boldsymbol{\ell}}{\mathrm{d}t} = (\rho^{\mathrm{T}}\rho\lambda^{\mathrm{T}} - \lambda^{\mathrm{T}}\lambda\rho^{\mathrm{T}})\gamma^{\mathrm{T}}\boldsymbol{v}'' - (\mathbb{1} - \rho^{\mathrm{T}}\rho\lambda^{\mathrm{T}}\lambda)\left(\frac{\partial \boldsymbol{F}}{\partial \boldsymbol{\ell}}\right)^{-1}\frac{\partial \boldsymbol{F}}{\partial \boldsymbol{L}}\frac{\mathrm{d}\boldsymbol{L}}{\mathrm{d}t}. \tag{24}$$

We finally use equations (4), (15) and (18) to eliminate $\boldsymbol{f}$, $\rho\boldsymbol{v}^{\mathrm{l}}$ and $\lambda\boldsymbol{v}^{\mathrm{r}}$ in equations (19) and (24). This yields

$$\frac{\mathrm{d}\boldsymbol{L}}{\mathrm{d}t} = (\rho^{\mathrm{T}} - \lambda^{\mathrm{T}})\Pi'\boldsymbol{V}'[\Pi'(\lambda - \rho)\boldsymbol{F}(\boldsymbol{\ell}, \boldsymbol{L})], \tag{25a}$$

$$\begin{aligned}\frac{\mathrm{d}\boldsymbol{\ell}}{\mathrm{d}t} = &-\left(\frac{\partial \boldsymbol{F}}{\partial \boldsymbol{\ell}}\right)^{-1}\frac{\partial \boldsymbol{F}}{\partial \boldsymbol{L}}(\rho^{\mathrm{T}}\rho - \lambda^{\mathrm{T}}\lambda)(\rho^{\mathrm{T}} + \lambda^{\mathrm{T}})\Pi'\boldsymbol{V}'[\Pi'(\lambda - \rho)\boldsymbol{F}(\boldsymbol{\ell}, \boldsymbol{L})] \\ &+ (\rho^{\mathrm{T}}\rho\lambda^{\mathrm{T}} - \lambda^{\mathrm{T}}\lambda\rho^{\mathrm{T}})\gamma^{\mathrm{T}}\boldsymbol{v}''_{\mathrm{s}}(\boldsymbol{\ell}, \boldsymbol{L}),\end{aligned} \tag{25b}$$

where the nonlinear vector function $\boldsymbol{v}''_{\mathrm{s}}(\boldsymbol{\ell}, \boldsymbol{L})$ is the solution to the linear (in $\boldsymbol{v}''$) system of equations formed by equation (1) and the following vector equation, obtained by combining equations (12) and (15), then differentiating with respect to time and inserting equations (25) into the result:

$$\gamma(\rho - \lambda)\frac{\partial \boldsymbol{F}}{\partial \boldsymbol{\ell}}(\rho^{\mathrm{T}}\rho\lambda^{\mathrm{T}} - \lambda^{\mathrm{T}}\lambda\rho^{\mathrm{T}})\gamma^{\mathrm{T}}\boldsymbol{v}'' = \gamma(\rho - \lambda)\frac{\partial \boldsymbol{F}}{\partial \boldsymbol{L}}(\rho^{\mathrm{T}}\rho\lambda^{\mathrm{T}} - \lambda^{\mathrm{T}}\lambda\rho^{\mathrm{T}})\Pi'\boldsymbol{V}'[\Pi'(\lambda - \rho)\boldsymbol{F}(\boldsymbol{\ell}, \boldsymbol{L})]. \tag{26}$$

Equation (26), just like equation (12), has only $n'' - 1$ independent scalar equations, and supplementing it with equation (1) thus results in a complete set of equations for $\boldsymbol{v}''_{\mathrm{s}}$. Finally, supplementing equations (1), (25) and (26) with an initial condition $[\boldsymbol{\ell}(t = 0), \boldsymbol{L}(t = 0)]$ completely specifies the dynamics of a bundle of arbitrary geometry.

[5] Mechanical stability imposes that $\partial F/\partial \ell$ is always strictly negative, making the matrix $\partial \boldsymbol{F}/\partial \boldsymbol{\ell}$ invertible.

3. Situations without telescopic deformation

We now ask under what conditions contraction occurs. We are interested in bundles much longer than the size of any single one of their constituents (F-actin or motor). Significant contraction of such a bundle requires that it contracts throughout its length, as opposed to, e.g., contracting at its extremities while the bulk of the bundle retains a constant length. We thus focus on 'telescopic deformation', whereby the end-to-end velocity of a bundle contracting under vanishing external load is proportional to its length. This constitutes the standard behavior of contractile actomyosin structures *in vivo* [1, 24–26] and *in vitro* [13]. Telescopic deformation is characteristic of systems formed by a serial arrangement of many independently deforming elements, often referred to as 'contractile units' [13, 25, 26].

Here we demonstrate two requirements for telescopic deformation. In section 3.1, we show that it cannot arise if the motors all have identical force–velocity relationships. Section 3.2 then tackles situations where motors with different force–velocity relationships are present. In that case, we prove that bundles lacking polarity organization comprised of linearly elastic (i.e. rigid) filaments do not undergo telescopic deformation. Such rigid filament units represent situations where the filament persistence length is very large (e.g. bundles of microtubules and kinesin oligomers) or when the filament units themselves are very short (e.g. strongly cross-linked bundles, where the spacing between two junctions is small).

To completely determine the bundle dynamics, we need to specify an initial condition $[\boldsymbol{\ell}(t=0), \boldsymbol{L}(t=0)]$. We thus choose an arbitrary vector $\boldsymbol{L}_0$ of length n and impose $\boldsymbol{L}(t=0) = \boldsymbol{L}_0$. To avoid confusion between the effects of motor-generated stresses, which are relevant for contractility, and those of bundle prestress, which are not, we consider bundles that are initially stress-free:

$$\boldsymbol{f}(t=0) = \boldsymbol{F}[\boldsymbol{\ell}(t=0), \boldsymbol{L}(t=0)] = 0. \tag{27}$$

This imposes $\boldsymbol{\ell}(t=0) = \boldsymbol{\ell}_0$, where $\boldsymbol{\ell}_0$ is the solution of the equation $\boldsymbol{F}(\boldsymbol{\ell}_0, \boldsymbol{L}_0) = 0$ and thus completely specifies the bundle initial condition.

3.1. Motors with identical force–velocity relationships

In a bundle where the motors have identical force–velocity relationships, the junction units have identical spontaneous sliding velocities v^* in the absence of applied force. Defining $\boldsymbol{v}^*$ as the length n' vector with all its components equal to v^*, we can thus write

$$\boldsymbol{V}'(\boldsymbol{f}=0) = \boldsymbol{v}^*. \tag{28}$$

We now demonstrate that under this assumption, all linker units are immobile throughout the dynamics and all right-pointing filaments undergo a uniform translation with constant velocity v^*, while left-pointing filaments translate with $-v^*$.

We define the set of functions $[\boldsymbol{\ell}^*(t), \boldsymbol{L}^*(t)]$ by

$$\boldsymbol{L}^*(t) = \boldsymbol{L}_0 + (\rho^{\mathrm{T}} - \lambda^{\mathrm{T}})\Pi'\boldsymbol{v}^* t \tag{29}$$

and by defining $\boldsymbol{\ell}^*(t)$ as the solution of $\boldsymbol{F}[\boldsymbol{\ell}^*(t), \boldsymbol{L}^*(t)] = 0$. This set manifestly satisfies the initial condition $[\boldsymbol{\ell}_0, \boldsymbol{L}_0]$ chosen above. Inserting $[\boldsymbol{\ell}^*(t), \boldsymbol{L}^*(t)]$ into equations (25), we further verify that these functions satisfy the equations of motion, implying that they describe the dynamics of the bundle. Using equations (18) and (26), we find that $\boldsymbol{v}'' = 0$ and

$\rho \boldsymbol{v}^{\mathrm{l}} = \lambda \boldsymbol{v}^{\mathrm{r}} = \Pi' \boldsymbol{v}^*$ for all times, thus confirming that linker units are immobile and that the velocities associated with right- and left-pointing actin are v^* and $-v^*$, respectively.

In this regime, the maximum relative speed between any two actin filament units is $2|v^*|$ irrespective of bundle geometry. Defining the contraction velocity of the bundle as the difference between the velocities of its leftmost and rightmost filaments, this implies that the contraction velocity cannot exceed the constant $2|v^*|$. It is thus impossible for the contraction velocity to scale linearly with bundle length, and telescopic contractility does not occur. Instead, filaments are segregated according to polarity, as observed experimentally in [27]. Note that this result does not require the bundle to be disordered.

3.2. *Disordered bundles with linearly elastic filaments*

In a bundle with arbitrary force–velocity relationships, the reasoning of the previous section does not apply, and some amount of contraction or extension is generally present. We thus ask whether bundles contract *on average*, and find that they do only if filament polarities are organized across the bundles or if the filaments display nonlinear elastic behavior.

To prove this statement, we first give a mathematical description of bundles devoid of both polarity organization and filament nonlinear elastic behavior (section 3.2.1) and then use equations (25) and (26) to show that such bundles do not contract (section 3.2.2).

3.2.1. Mathematical formulation. Consider an arbitrary bundle, which we denote by B. Bundle B is fully characterized by specifying matrices λ, ρ, Π, γ, the force–velocity functions $\boldsymbol{V}'$ and the initial condition $\boldsymbol{L}_0$. Therefore, a population of bundles is fully characterized by specifying the distribution $\mathcal{P}(B) = \mathcal{P}(\lambda, \rho, \Pi, \gamma, \boldsymbol{V}', \boldsymbol{L}_0)$ of the frequencies at which any possible bundle B arises in the population. For a population without any polarization organization, $\mathcal{P}(B)$ must be independent of Π, implying in particular that it is invariant under polarity reversal:

$$\mathcal{P}(\lambda, \rho, \Pi, \gamma, \boldsymbol{V}', \boldsymbol{L}_0) = \mathcal{P}(\lambda, \rho, -\Pi, \gamma, \boldsymbol{V}', \boldsymbol{L}_0). \tag{30}$$

This relationship clearly does not apply to a population of sarcomeres. Indeed, in a sarcomere, static cross-linkers are restricted to the barbed ends of F-actin, while active, mobile motors are found at the pointed ends. Thus the polarity-reversed image of a sarcomere is not a sarcomere; actually, inverting the polarities of filaments in figure 1(a) results in an extensile, not contractile, structure. Assumption of equation (30) excludes sarcomeric contractility from our discussion below.

We further assume that filament units exhibit linear elastic behavior, which reads

$$\boldsymbol{F}(\boldsymbol{\ell}, \boldsymbol{L}) = \frac{\partial \boldsymbol{F}}{\partial \boldsymbol{\ell}}(\boldsymbol{\ell} - \boldsymbol{\ell}_0) + \frac{\partial \boldsymbol{F}}{\partial \boldsymbol{L}}(\boldsymbol{L} - \boldsymbol{L}_0), \tag{31a}$$

where $\partial F/\partial \ell$ and $\partial F/\partial L$ are constants, i.e.

$$\frac{\mathrm{d}}{\mathrm{d}t}\left(\frac{\partial \boldsymbol{F}}{\partial \boldsymbol{\ell}}\right) = \frac{\mathrm{d}}{\mathrm{d}t}\left(\frac{\partial \boldsymbol{F}}{\partial \boldsymbol{L}}\right) = 0. \tag{31b}$$

This assumption is a good description of very stiff filaments, where $\ell_i = L_i$ for any filament unit i. Indeed, such filaments can be described by choosing the force–extension relationship

$$F(\ell_i, L_i) = K(\ell_i - L_i), \tag{32}$$

and enforcing the limit $K \to +\infty$. Here K is a constant and therefore equation (32) satisfies equations (31).

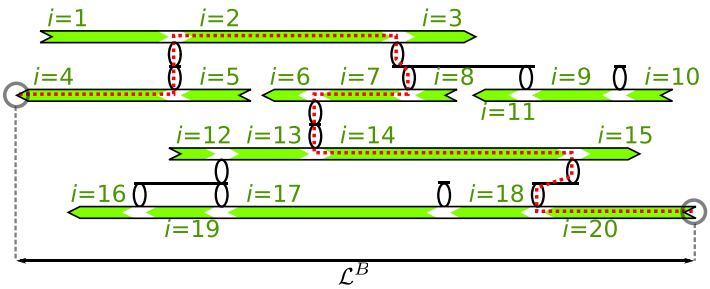

Figure 4. Example of a path (red dotted line), as discussed in section 3.2.2. The leftmost and rightmost points of the bundle are labelled by gray circles. In this example, $\epsilon_2^B = \epsilon_4^B = \epsilon_{14}^B = \epsilon_{20}^B = -\epsilon_7^B = 1$ and all other ϵ_i^Bs are equal to zero. As a consequence, equation (33) reads $\mathrm{d}\mathcal{L}^B/\mathrm{d}t = \mathrm{d}(\ell_4^B + \ell_2^B - \ell_7^B + \ell_{14}^B + \ell_{20}^B)/\mathrm{d}t$.

3.2.2. Proof of the property. To determine whether a bundle $B = \{\lambda, \rho, \Pi, \gamma, \boldsymbol{V}', \boldsymbol{L}_0\}$ is contractile or extensile, we imagine labeling its leftmost and rightmost points, and ask whether the distance $\mathcal{L}^B$ between these two labels tends to increase or decrease with time. To calculate $\mathcal{L}^B$, we choose a path along the bundle's linker and filament units going from the left label to the right label as pictured in figure 4. We define ϵ_i^B as equal to 1 if the path considered crosses filament unit i from left to right, to -1 if it crosses it from right to left and to 0 otherwise (see the caption of figure 4). The contraction velocity of the bundle can then be defined as

$$\frac{\mathrm{d}\mathcal{L}^B}{\mathrm{d}t} = \sum_{i=1}^{n} \epsilon_i^B \frac{\mathrm{d}\ell_i^B}{\mathrm{d}t}. \tag{33}$$

We use the following notation to refer to the solution of the equations of motion for bundle B:

$$\boldsymbol{L}^B(t) = \boldsymbol{L}_0 + \Delta\boldsymbol{L}^B(t), \tag{34a}$$

$$\boldsymbol{\ell}^B(t) = \boldsymbol{\ell}_0 + \Delta\boldsymbol{\ell}^B(t). \tag{34b}$$

We now introduce bundle $\tilde{B}$ as the polarity-reversed image of B, i.e. $\tilde{B} = \{\lambda, \rho, -\Pi, \gamma, \boldsymbol{V}', \boldsymbol{L}_0\}$. Substituting equations (31) into equations (25) and (26), we find that the dynamics of $\tilde{B}$ satisfies

$$\Delta\boldsymbol{L}^{\tilde{B}}(t) = -\Delta\boldsymbol{L}^B(t), \tag{35a}$$

$$\Delta\boldsymbol{\ell}^{\tilde{B}}(t) = -\Delta\boldsymbol{\ell}^B(t). \tag{35b}$$

Combining this with equations (33) and (34) while using the path $\epsilon_i^{\tilde{B}} = \epsilon_i^B$ to assess the contraction of $\tilde{B}$, we find that

$$\frac{\mathrm{d}\mathcal{L}^{\tilde{B}}}{\mathrm{d}t} = -\frac{\mathrm{d}\mathcal{L}^B}{\mathrm{d}t}. \tag{36}$$

We finally calculate the average contraction velocity over a population of bundles as

$$\left\langle \frac{\mathrm{d}\mathcal{L}}{\mathrm{d}t} \right\rangle = \sum_B \mathcal{P}(B) \frac{\mathrm{d}\mathcal{L}^B}{\mathrm{d}t}, \tag{37}$$

where the sum runs over all possible bundles. Reorganizing this sum, we find that

$$\left\langle \frac{\mathrm{d}\mathcal{L}}{\mathrm{d}t} \right\rangle = \frac{1}{2} \sum_B \left[\mathcal{P}(B) \frac{\mathrm{d}\mathcal{L}^B}{\mathrm{d}t} + \mathcal{P}(\tilde{B}) \frac{\mathrm{d}\mathcal{L}^{\tilde{B}}}{\mathrm{d}t} \right] = \frac{1}{2} \sum_B \mathcal{P}(B) \left(\frac{\mathrm{d}\mathcal{L}^B}{\mathrm{d}t} + \frac{\mathrm{d}\mathcal{L}^{\tilde{B}}}{\mathrm{d}t} \right) = 0, \tag{38}$$

where equations (30) and (36) are used to derive the second and third equalities, respectively. Equation (38) demonstrates that bundles without polarity organization or nonlinear elastic behavior do not contract or extend on average. This result does not depend on bundle structure or the form of the motor force–velocity relationships, and can easily be generalized to bundles pinned to a rigid substrate, or to include friction of the linker or filament units with the solvent. Mean-field modeling of dilute actomyosin gels with rigid filaments suggests that this symmetry-based reasoning could have a three-dimensional counterpart [23]. However, geometrical nonlinearities in two or more dimensions can take on the role played by elastic nonlinearities in one-dimensional bundles, thus enabling contraction in disordered networks of rigid filaments [28].

4. Discussion

In this paper, we consider bundles of sliding motors and filaments with arbitrary geometries and motor force–velocity relationships and show that their contractility requires

1. non-identical motors and
2. either
   (a) polarity organization or
   (b) nonlinear elastic response of the filaments.

While our model is framed in terms of F-actin and myosin for clarity, our results are much more general and could equally apply to bundles comprised of other types of motors and filaments (e.g. kinesins and microtubules). Our description includes as a special case the well-understood contractility of striated muscle sarcomeres (figure 1(a)). Their architecture includes both identical myosin thick filaments and passive cross-linkers (which are mathematically equivalent to motors with velocity zero), thus satisfying condition (1). They, moreover, have a distinctive polarity organization and thereby fulfill condition (2a). Similarly, bundles with motors whose velocities depend on their position relative to the filaments [19–23] generically break polarity-reversal symmetry, which results in polarity organization.

Besides establishing the requirements for contractility, the formalism presented here can describe the dynamics of a wide range of contractile bundles. For instance, straightforward numerical simulations of equations (25) and (26) could be used to describe bundle deformation as a function of the initial arrangement of the filament and motors. Comparing these predictions to experimental observations while varying these initial parameters could yield insight into the architecture of the bundles, which is currently lacking. Although such a study is beyond the scope of this work, a simplified version of our formalism still successfully predicts the onset of their contraction [29].

Whereas the model used here is designed to describe a large class of contractile bundles, some of our assumptions are particularly appropriate for describing the reconstituted bundles of [13]. F-actin is phalloidin-stabilized in this system, implying that no actin polymerization–depolymerization takes place; myosin thick filaments are much shorter ($\simeq$300 nm) and thicker ($\simeq$50 nm) than F-actin ($\simeq 5\,\mu$m and $\simeq$5 nm, respectively), justifying

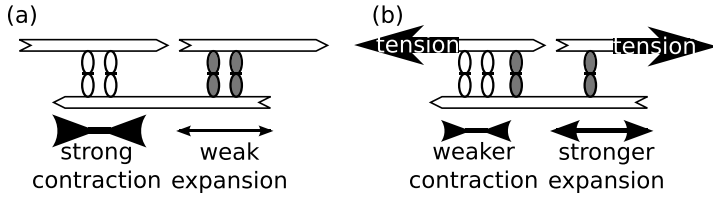

Figure 5. The Fenn effect impedes bundle contractility. (a) Simple contractile bundle comprised of fast (light) and slow (dark) motors. Double-headed arrows indicate local contraction or expansion due to the movement of the motors relative to the filaments (figure 1(b)). (b) As tension builds following contraction, the motors detach and reorganize and contractility diminishes.

our assumption that they behave as rigid objects; and myosin thick filaments do not detach from the bundle on the time scales relevant for contraction, suggesting that the filament–motor attachment–detachment dynamics are inessential for contractility. Indeed, we show elsewhere that attachment–detachment can limit contractility under low myosin conditions [29].

Going beyond the specifics of the system studied in [13], it is interesting to discuss bundles where this attachment–detachment dynamics is not negligible. In the simplest such situation, motors undergo attachment and detachment at a constant rate, which tends to randomize their distribution in a filament polarity-independent manner. This fails to break the polarity-reversal symmetry discussed in this paper, and the resulting requirements for contractility are unchanged.

A more interesting question is to ask whether contractility could arise from the load-dependent detachment of myosin motors. Specifically, the detachment rate of myosin motors decreases under increasing load, a tendency known as the 'Fenn effect' [30]. To assess its influence on contractility, we consider the simple bundle of rigid filaments illustrated in figure 5(a). This bundle comprises a contracting and an expanding region similar to those of figure 1(b). When faster motors happen to be concentrated in the contracting region, this bundle is contractile. Assuming that its ends are fixed, the bundle comes under tensile force during contraction. As a consequence, its expanding region comes under negative load and the motors there tend to detach. Conversely, the motors in the contracting region experience a positive load and tend to hold on to the filaments. On average, detached motors thus tend to diffuse from the expanding to the contracting region (figure 5(b)). The reduced number of motors in the expanding region implies that its resistance to the applied tension decreases, thus increasing its expansion rate. As the contracting region tends to recruit the slower motors from the expanding region, its contraction rate decreases. Overall, the Fenn effect thus tends to suppress contractile configurations rather than amplify them. This suggests that the Fenn effect cannot generate contractility in the absence of polarity organization or filament nonlinear elastic response.

The requirements derived in this paper offer insight into the contractility of actomyosin bundles without sarcomere-like organization, for which no established contraction mechanism exists. As they do not satisfy condition (2a), we propose that they contract by fulfilling conditions (1) and (2b) [29]. Consider two antiparallel filaments interacting through several different motors with distinct speeds (figure 6(a)). As motors start to move relative to the filaments, stresses build up in sections of the filament flanked by motors with different speeds. When the flanking motor proximal to the barbed end is faster than that proximal to the pointed end, compression arises. When it is slower, tension arises. F-actin responds nonlinearly to

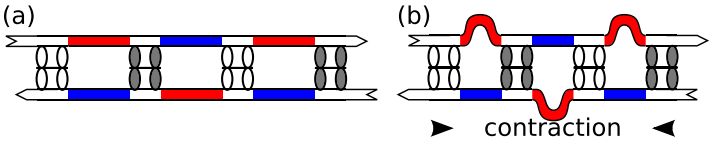

Figure 6. Filament buckling as a mechanism of bundle contractility. (a) The presence of fast (white) and slow (gray) motors generically induces compressive (red) and extensile (blue) stresses in filaments. (b) Buckling of the compressed filaments leads to an overall shortening of the bundle. Buckling of filament units of length $L_i = 500\,\mathrm{nm}$ occurs for compressive forces of order $k_\mathrm{B}T\,\ell_\mathrm{p}/L_i^2 \simeq 0.16\,\mathrm{pN}$, where $\ell_\mathrm{p} \simeq 10\,\mu\mathrm{m}$ is the F-actin persistence length. Myosin thick filaments typically exert forces of several piconewtons [33], which is sufficient for inducing buckling, but remains smaller than the tension required to break F-actin ($\simeq$100 pN [34]).

these stresses by buckling under compression while resisting extension, which has previously been proposed to play a role in actomyosin contraction [31]. Following the buckling of the compressed filament sections, fast motors are free to move quickly while the others move slowly. This results in the growth of compressed sections and the shrinkage of extended ones, and thus in overall bundle contraction (figure 6(b)). Experimental observations suggest that this mechanism could be at the origin of contraction in reconstituted actomyosin bundles [29] and that F-actin buckling can occur in cells [32]. These results offer a new, interesting perspective on the mechanisms underlying actomyosin bundle contraction *in vivo*.

Acknowledgments

We thank Yitzhak Rabin, Todd Thoresen and Tom Witten for inspiring discussions. This work was supported by NSF DMR-MRSEC grant no. 0820054.

References

[1] Alberts B, Bray D, Johnson A, Lewis J, Raff M, Roberts K and Walter P 1998 *Essential Cell Biology* (New York: Garland)

[2] Peterson L J, Rajfur Z, Maddox A S, Freel C D, Chen Y, Edlund M, Otey C and Burridge K 2004 Simultaneous stretching and contraction of stress fibers *in vivo Mol. Biol. Cell* **15** 3497–508

[3] Fay F S, Fujiwara K, Rees D D and Fogarty K E 1983 Distribution of alpha-actinin in single isolated smooth muscle cells *J. Cell Biol.* **96** 783–95

[4] Heath J P 1983 Behaviour and structure of the leading lamella in moving fibroblasts. I. Occurrence and centripetal movement of arc-shaped microfilament bundles beneath the dorsal cell surface *J. Cell Sci.* **60** 331–54

[5] Cramer L P, Siebert M and Mitchison T J 1997 Identification of novel graded polarity actin filament bundles in locomoting heart fibroblasts: implications for the generation of motile force *J. Cell Biol.* **136** 1287–305

[6] Medalia O, Weber I, Frangakis A S, Nicastro D, Gerisch G and Baumeister W 2002 Macromolecular architecture in eukaryotic cells visualized by cryoelectron tomography *Science* **298** 1209–13

[7] Verkhovsky A B, Svitkina T M and Borisy G G 1995 Myosin II filament assemblies in the active lamella of fibroblasts: their morphogenesis and role in the formation of actin filament bundles *J. Cell Biol.* **131** 989–1002

[8] Szent-Györgyi A 1947 *Chemistry of Muscular Contraction* (New York: Academic)
[9] Janson L W, Kolega J and Taylor D L 1991 Modulation of contraction by gelation/solation in a reconstituted motile model *J. Cell Biol.* **114** 1005–15
[10] Mizuno D, Tardin C, Schmidt C F and Mackintosh F C 2007 Nonequilibrium mechanics of active cytoskeletal networks *Science* **315** 370–3
[11] Bendix P M, Koenderink G H, Cuvelier D, Dogic Z, Koeleman B N, Brieher W M, Field C M, Mahadevan L and Weitz D A 2008 A quantitative analysis of contractility in active cytoskeletal protein networks *Biophys. J.* **94** 3126–36
[12] Koenderink G H, Dogic Z, Nakamura F, Bendix P M, MacKintosh F C, Hartwig J H, Stossel T P and Weitz D A 2009 An active biopolymer network controlled by molecular motors *Proc. Natl Acad. Sci. USA* **106** 15192–7
[13] Thoresen T, Lenz M and Gardel M L 2011 Reconstitution of contractile actomyosin bundles *Biophys. J.* **100** 2698–705
[14] Kruse K, Zumdieck A and Jülicher F 2003 Continuum theory of contractile fibres *Europhys. Lett.* **64** 716–22
[15] Kruse K, Joanny J-F, Jülicher F, Prost J and Sekimoto K 2004 Asters, vortices, and rotating spirals in active gels of polar filaments *Phys. Rev. Lett.* **92** 078101
[16] Kruse K, Joanny J F, Jülicher F, Prost J and Sekimoto K 2005 Generic theory of active polar gels: a paradigm for cytoskeletal dynamics *Eur. Phys. J.* E **16** 5–16
[17] MacKintosh F C and Levine A J 2008 Nonequilibrium mechanics and dynamics of motor-activated gels *Phys. Rev. Lett.* **100** 018104
[18] Zemel A and Mogilner A 2009 Motor-induced sliding of microtubule and actin bundles *Phys. Chem. Chem. Phys.* **11** 4821–33
[19] Kruse K and Jülicher F 2000 Actively contracting bundles of polar filaments *Phys. Rev. Lett.* **85** 1778–81
[20] Kruse K and Jülicher F 2003 Self-organization and mechanical properties of active filament bundles *Phys. Rev.* E **67** 051913
[21] Liverpool T B and Marchetti M C 2003 Instabilities of isotropic solutions of active polar filaments *Phys. Rev. Lett.* **90** 138102
[22] Ziebert F and Zimmermann W 2005 Nonlinear competition between asters and stripes in filament-motor systems *Eur. Phys. J.* E **18** 41–54
[23] Liverpool T B and Marchetti M C 2005 Bridging the microscopic and the hydrodynamic in active filament solutions *Europhys. Lett.* **69** 846–52
[24] Bement W M and Capco D G 1991 Analysis of inducible contractile rings suggests a role for protein kinase C in embryonic cytokinesis and wound healing *Cell Motil. Cytoskeleton* **20** 145–57
[25] Herrera A M, McParland B E, Bienkowska A, Tait R, Paré P D and Seow C Y 2005 'Sarcomeres' of smooth muscle: functional characteristics and ultrastructural evidence *J. Cell Sci.* **118** 2381–92
[26] Carvalho A, Desai A and Oegema K 2009 Structural memory in the contractile ring makes the duration of cytokinesis independent of cell size *Cell* **137** 926–37
[27] Tanaka-Takiguchi Y, Kakei T, Tanimura A, Takagi A, Honda M, Hotani H and Takiguchi K 2004 The elongation and contraction of actin bundles are induced by double-headed myosins in a motor concentration-dependent manner *J. Mol. Biol.* **341** 467–76
[28] Dasanayake N L, Michalski P J and Carlsson A E 2011 General mechanism of actomyosin contractility *Phys. Rev. Lett.* **107** 118101
[29] Lenz M, Thoresen T, Gardel M L and Dinner A R 2012 Contractile units in disordered actomyosin bundles arise from F-actin buckling arXiv:1201.4110
[30] Veigel C, Molloy J E, Schmitz S and Kendrick-Jones J 2003 Load-dependent kinetics of force production by smooth muscle myosin measured with optical tweezers *Nature Cell Biol.* **5** 980–6
[31] Soares e Silva M, Depken M, Stuhrmann B, Korsten M, Mackintosh F C and Koenderink G H 2011 Active multistage coarsening of actin networks driven by myosin motors *Proc. Natl Acad. Sci. USA* **108** 9408–13

[32] Costa K D, Hucker W J and Yin F C-P 2002 Buckling of actin stress fibers: a new wrinkle in the cytoskeletal tapestry *Cell Motil. Cytoskeleton* **52** 266–74

[33] Molloy J E, Burns J E, Kendrick-Jones J, Tregear R T and White D C S 1995 Movement and force produced by a single myosin head *Nature* **378** 209–12

[34] Kishino A and Yanagida T 1988 Force measurements by micromanipulation of a single actin filament by glass needles *Nature* **334** 74–6